PHYSICAL REVIEW B VOLUME 45, NUMBER 11 15 MARCH 1992-I

Carbon fibers based on C_{60} and their symmetry

M.S. Dresselhaus
Department of Electrical Engineering and Computer Science and Department of Physics, Massachusetts Institute of Technology, Cambridge, Massachusetts 02139

G. Dresselhaus
Francis Bitter National Magnet Laboratory, Massachusetts Institute of Technology, Cambridge, Massachusetts 02139

Riichiro Saito*
Department of Physics, Massachusetts Institute of Technology, Cambridge, Massachusetts 02139
(Received 24 September 1991; revised manuscript received 19 November 1991)

Carbon fibers based on the recently discovered fullerenes are proposed and their symmetry properties examined with respect to Raman- and infrared-active vibrational modes. Such carbon fibers are of interest as approximating the smallest possible diameter for a vapor-grown carbon fiber, and can be used for model calculations for the structure and properties of this limiting case of a carbon fiber.

I. INTRODUCTION

A great deal of interest has recently been generated by C_{60} molecules, by their unique symmetry and by their special properties.[1–4] Closely related to the C_{60} molecules are higher-order fullerenes such as C_{70} and C_{78} which have also been reported. We can think of some of these higher-order fullerenes as the first members of a series of fullerenes such as C_{60+10j}, C_{60+18j}, and C_{78+4j} (for j an integer $j \geq 1$) which form single-layer carbon fibers in the limit of large j.[5] One can envisage fibers formed along a fivefold axis, a threefold axis, and a twofold axis relative to the C_{60} molecule. These fiber categories are discussed below.

In analogy to the name of "bucky balls" that has been used for the C_{60} molecules, one might call the fibers based on C_{60} "bucky fibers," but we will use the more formal and descriptive name of graphene tubule, a single layer of the honeycomb graphite structure that is rolled up in the form of a cylinder. In relation to carbon fibers that are grown commercially or on a laboratory scale,[6] we shall see that, because of their annular structure, the graphene tubules relate closely to carbon fibers grown from a carbon nucleation site (as discussed below) in the vapor phase. Though the fullerenes would be expected to grow directly from the vapor phase, probably from a carbon-based nucleation site, the conventional fibers require use of a small transition-metal particle (~100 Å diameter) as a catalyst.[7,8] The larger diameter of the conventional vapor-grown carbon fibers allows one to deposit multiple cylindrical layers in a turbostratic arrangement with respect to each other.[9] Heat treatment of these vapor-grown turbostratic fibers can produce graphitic registry between graphene layers, but then the fiber morphology changes to a polyhedral rather than a circular cross section.[10] The special interest of graphene tubules in relation to the broad field of carbon-fiber science and technology is the fact that a graphene tubule can be considered as an approximation to the smallest possible diameter for a carbon fiber, only one atomic layer thick. Graphene tubules are thus of interest for model calculations for structure-properties relations. In this paper we consider the symmetry properties of various types of carbon fibers based on C_{60}, particularly those based on a fivefold or a threefold axis, because of the higher symmetry of these fibers.

II. CLASSIFICATION OF GRAPHENE TUBULES

There are three major classifications of the graphene tubules, depending on whether they relate to a fivefold, a threefold, or a twofold axis relative to the C_{60} molecule. Generally speaking, all graphene tubules consist of a graphene sheet (in the graphite literature[6] an isolated monolayer of the graphite crystal structure normal to the c axis is called a graphene sheet) rolled up in one dimension to form a cylinder with top and bottom edges that fit perfectly on to a cap at either end, the caps being formed by appropriately cutting the C_{60} molecule in half (see Fig. 1). Both the C_{60+10j} and C_{60+18j} (for $j = 1, 2, \ldots$) types of graphene tubules can be considered as a limiting case of a vapor-grown carbon fiber[11] with a monolayer thickness.

A. Fibers with fivefold symmetry

To be explicit, let us first consider the fiber formed along a fivefold axis, which is the easiest to visualize and can be represented by the formula C_{60+10j} where j is a positive integer. We can think of this C_{60+10j} fiber as composed of a rolled up graphene sheet containing j rows of "armchair" hexagons, each row containing five

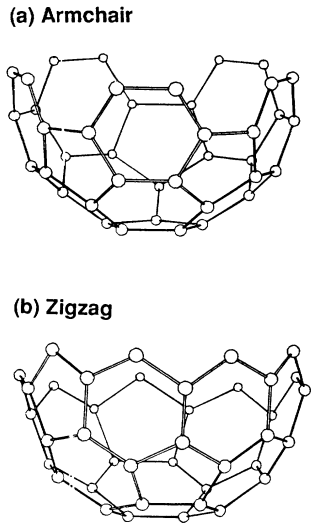

FIG. 1. The caps to graphene tubules formed by cutting the C_{60} molecule along the equatorial plane: (a) the armchair cap normal to a fivefold axis; (b) the zigzag cap normal to a threefold axis.

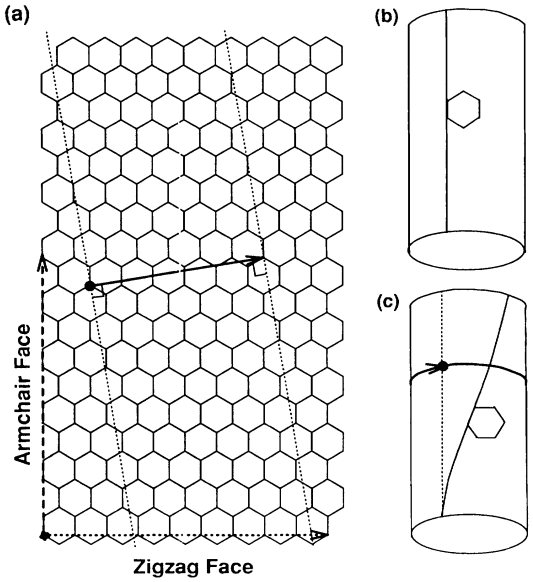

FIG. 2. The "graphene tubules" are based on a graphene sheet and are uniquely determined by the lattice vectors shown in (a). The lattice vector shown by the long-dashed vector forms an armchair graphene tubule. The heavy dotted vector defines the zigzag graphene tubule. To make a tubule, the graphene layer is rolled to form a cylinder as shown in (b) and (c) by joining one end of the vector to the other end, so that the vector is π times the cylinder diameter. The solid arrow defines a chiral fiber which is rolled up as indicated in (c). For the example shown, the diameter of the chiral fiber indicated by the solid arrow in (a) is 4.52 Å which is expected to be smaller than any stable fiber. The diameter of the castellated-hexagon and zigzag fibers which join perfectly to the caps in Fig. 1 are 6.83 Å and 7.08 Å, respectively.

full "armchairs" [see Fig. 2(a) where the vertical dashed vector indicates the size of this armchair row]. These rows of hexagons are joined at their zigzag ends to form a cylinder with a fivefold periodic-boundary condition. The ten carbon atoms at the top of the first row of armchair hexagons [see Fig. 2(a)] become identical with the carbon atoms to which they join on the cap in Fig. 1(a); likewise for the ten armchair atoms at the bottom of the last row of armchair hexagons in the figure. Therefore ten additional carbon atoms are introduced per row, as illustrated in Fig. 2(a). The top and bottom of the resulting cylinder [Fig. 2(b)] are joined to caps formed by cutting the C_{60} molecule along the edges closest to the equator, normal to a fivefold axis [see Fig. 1(a)]. The assembly of the cylinder and the two end caps form the C_{60+10j} (for $j = 1, 2, \ldots$) fiber. The cap is significant for nucleating the growth of the fiber.

In addition to the cylindrical arrangement with fivefold symmetry described above, fibers with a fivefold screw axis can be envisioned by joining the zigzag edges of armchair hexagons of rows separated by j' rows, thus giving rise to a left- or right-handed pitch of $\sqrt{3}j'/15$ [see Fig. 2(c)]. However, such chiral fibers would not fit perfectly to the caps formed directly from the C_{60} molecules. Because of their lower symmetry, we do not discuss in detail the symmetry of chiral fibers.

B. Fibers with threefold symmetry

Closely related to the C_{60+10j} fiber based on a fivefold axis is the C_{60+18j} fiber which is based on a threefold axis and consists of cylindrical tubes formed by j (where $j = 1, 2, \ldots$) rows of nine zigzag hexagons [see Fig. 2(a) where the heavy dashed vector indicates the length of the zigzag row and the rolled tubule in Fig. 2(b)]. The armchair edges of the j rows are in this case joined together to form a cylinder [similar to that shown in Fig. 2(b)] which is joined at the two ends to caps formed by cutting along the zigzag equatorial edges normal to a threefold axis [see Fig. 1(b)]. The nine zigzag hexagons can in fact be thought to consist of three groups of three zigzag hexagons, two of which fit on to hexagons and one fits on to a pentagon. Each row of nine zigzag hexagons introduces 18 new carbon atoms. The edges of the nine zigzag hexagons fit perfectly on to the hemispherical zigzag caps normal to a threefold axis. The assembly of the cylinder and the two caps form the C_{60+18j} (for $j = 1, 2, \ldots$) fiber series.

Since the adjacent rows of zigzag hexagons are inequivalent, chiral fibers can be formed by joining armchair edges shifted by $2j'$ rows [see Fig. 2(c)]. These chiral fibers correspond to right- or left-handed pitches of $\sqrt{3}j'/9$. As for the case of fivefold chiral cylinders, the threefold chiral cylinders do not fit perfectly on to the caps formed directly by cutting the C_{60} molecules into two halves.

C. Fibers with twofold symmetry

Labastie *et al.*[12] have reported that quasicylindrical structures with a chiral arrangement of hexagons on the

cylindrical surface can be generated parallel to a twofold axis with a 22-Å circumference and a $\sqrt{3}/9$ pitch. These authors show that for their C_{76+4m} chiral fibers, the lower cap has to be rotated by 40° each time a pair of hexagons are added, where the twist angle is $40m°$, $m = 1, \ldots, 9$. Since chirality is necessary to join the cylindrical shells to the caps, the symmetry is low and group theory is less useful than for the other fibers discussed in this paper.

D. Generalized chiral fibers

The chirality and the fiber diameter are uniquely specified by the solid vector in Fig. 2(a) which connects two crystallographically equivalent sites. The cylinder is formed by connecting together the two ends of the solid vector and the joint is made along the two lightly dotted lines in the figure. The chiral fiber thus generated has no distortion of bond angles other than the cylindrical curvature of the fiber. This curvature is somewhat different from that occurring in the armchair and zigzag fibers (which also differ slightly from each other). This generalized description of chiral fibers includes a range of pitches, extending from the armchair (dashed vector) to the zigzag (heavy dotted vector) fibers, which form limiting cases for one chiral sense. The other chirality is obtained by going from the heavy dotted zigzag vector to the negative of the armchair vector.

III. SYMMETRY CONSIDERATIONS

The symmetries of the three fiber types discussed above differ from one another since each is based on a different axis of highest symmetry. Below we develop the group theory for fibers based on a fivefold axis and on a threefold axis.

A. Group theory

1. Fivefold axis

Consider first the symmetry properties of the fibers based on the fivefold axis and no chirality. Here we need to distinguish the C_{60+20j} fibers which have inversion symmetry (D_{5d}) and an even number of armchair rows of carbon atoms from the C_{50+20j} fibers which have mirror plane symmetry (D_{5h}) and an odd number of armchair rows in their cylinders. The point group D_5 forms a subgroup for each of these fiber types and is also a subgroup of the icosahedral group I_h (see Table I). The higher symmetries for the two varieties of C_{60+10j} ($j = 1, 2, \ldots$) fibers are found by taking the appropriate direct products

$$D_{5d} = D_5 \otimes i \tag{1}$$

and

$$D_{5h} = D_5 \otimes \sigma_h . \tag{2}$$

Using the character tables for each of these groups (see Tables II and III for the characters and basis functions for D_{5d} and D_{5h}, respectively), we form the equivalence transformation $\chi^{\text{atom sites}}$ for each of the distinct groupings of carbon atoms as given in Tables IV and V, respectively. In the determination of $\chi^{\text{atom sites}}$ in Table IV we use the groupings of the C_{60+20j} molecule

$$C_{10}(\text{cap}^0) + C_{10}(\text{cap}^1) + (2+j)C_{20}(\text{layer}) \tag{3}$$

so that the pentagons at either end of the fivefold axis are out of phase by 36° and are related by the inversion operation, as is also the case for the C_{60} molecule itself. We consider each of the caps to contain 30 carbon atoms, and the cylindrical section to contain $20j$ carbon

TABLE I. Character table for the point group I_h, where $\tau = (1+\sqrt{5})/2$. Note C_5 and C_5^{-1} are in different classes, labeled $12C_5$ and $12C_5^2$ in the character table. Then $iC_5 = S_{10}^{-1}$ and $iC_5^{-1} = S_{10}$ are in the classes labeled $12S_{10}^3$ and $12S_{10}$, respectively. Also $iC_2 = \sigma_v$.

I_h	E	$12C_5$	$12C_5^2$	$20C_3$	$15C_2$	i	$12S_{10}^3$	$12S_{10}$	$20S_3$	$15\sigma_v$	Basis functions
A_g	+1	+1	+1	+1	+1	+1	+1	+1	+1	+1	$x^2+y^2+z^2$
F_{1g}	+3	$+\tau$	$1-\tau$	0	−1	+3	τ	$1-\tau$	0	−1	(R_x, R_y, R_z)
F_{2g}	+3	$1-\tau$	$+\tau$	0	−1	+3	$1-\tau$	τ	0	−1	
G_g	+4	−1	−1	+1	0	+4	−1	−1	+1	0	
H_g	+5	0	0	−1	+1	+5	0	0	−1	+1	$2z^2-x^2-y^2$, x^2-y^2, xy, xz, yz
A_u	+1	+1	+1	+1	+1	−1	−1	−1	−1	−1	
F_{1u}	+3	$+\tau$	$1-\tau$	0	−1	−3	$-\tau$	$\tau-1$	0	+1	(x, y, z)
F_{2u}	+3	$1-\tau$	$+\tau$	0	−1	−3	$\tau-1$	$-\tau$	0	+1	(x^3, y^3, z^3)
G_u	+4	−1	−1	+1	0	−4	+1	+1	−1	0	$x(z^2-y^2)$, $y(x^2-z^2)$, $z(y^2-x^2)$, xyz
H_u	+5	0	0	−1	+1	−5	0	0	+1	−1	

TABLE II. Character table for the point group D_{5d}. Note: $iC_5 = S_{10}^{-1}$ and $iC_5^2 = S_{10}$. Also $iC_2' = \sigma_d$. Note also that $\tau = (1+\sqrt{5})/2$ so that $\tau = -2\cos 2\alpha = -2\cos 4\pi/5$ and $\tau - 1 = 2\cos\alpha = 2\cos 2\pi/5$, where $\alpha = 2\pi/5 = 72°$.

D_{5d}	E	$2C_5$	$2C_5^2$	$5C_2'$	i	$2S_{10}^{-1}$	$2S_{10}$	$5\sigma_d$	Basis functions
A_{1g}	+1	+1	+1	+1	+1	+1	+1	+1	$(x^2+y^2), z^2$
A_{2g}	+1	+1	+1	−1	+1	+1	+1	−1	R_z
E_{1g}	+2	$\tau-1$	$-\tau$	0	+2	$\tau-1$	$-\tau$	0	$z(x+iy, x-iy)$, (R_x, R_y)
E_{2g}	+2	$-\tau$	$\tau-1$	0	+2	$-\tau$	$\tau-1$	0	$[(x+iy)^2, (x-iy)^2]$
A_{1u}	+1	+1	+1	+1	−1	−1	−1	−1	
A_{2u}	+1	+1	+1	−1	−1	−1	−1	+1	z
E_{1u}	+2	$\tau-1$	$-\tau$	0	−2	$1-\tau$	$+\tau$	0	$(x+iy, x-iy)$
E_{2u}	+2	$-\tau$	$\tau-1$	0	−2	$+\tau$	$1-\tau$	0	

TABLE III. Character table for the point group D_{5h}. Note that $\tau = (1+\sqrt{5})/2$ so that $\tau = -2\cos 2\alpha = -2\cos 4\pi/5$ and $\tau - 1 = 2\cos\alpha = 2\cos 2\pi/5$.

D_{5h}	E	$2C_5$	$2C_5^2$	$5C_2'$	σ_h	$2S_5$	$2S_5^3$	$5\sigma_v$	Basis functions
A_1'	+1	+1	+1	+1	+1	+1	+1	+1	x^2+y^2, z^2
A_2'	+1	+1	+1	−1	+1	+1	+1	−1	R_z
E_1'	+2	$\tau-1$	$-\tau$	0	+2	$\tau-1$	$-\tau$	0	(x,y), (xz^2, yz^2), $[x(x^2+y^2), y(x^2+y^2)]$
E_2'	+2	$-\tau$	$\tau-1$	0	+2	$-\tau$	$\tau-1$	0	(x^2-y^2, xy), $[y(3x^2-y^2), x(x^2-3y^2)]$
A_1''	+1	+1	+1	+1	−1	−1	−1	−1	
A_2''	+1	+1	+1	−1	−1	−1	−1	+1	z, z^3, $z(x^2+y^2)$
E_1''	+2	$\tau-1$	$-\tau$	0	−2	$1-\tau$	$+\tau$	0	(R_x, R_y), (xz, yz)
E_2''	+2	$-\tau$	$\tau-1$	0	−2	$+\tau$	$1-\tau$	0	$[xyz, z(x^2-y^2)]$

TABLE IV. $\chi^{\text{atom sites}}$ for the C_{80+20j} molecules for D_{5d} symmetry.

Site	E	$2C_5$	$2C_5^2$	$5C_2'$	i	$2S_{10}^{-1}$	$2S_{10}$	$5\sigma_d$	$\chi^{\text{atom sites}}$
$C_{10}(\text{cap}^0)$	10	0	0	0	0	0	0	2	$A_{1g}+E_{1g}+E_{2g}+A_{2u}+E_{1u}+E_{2u}$
$C_{10}(\text{cap}^1)$	10	0	0	0	0	0	0	2	$A_{1g}+E_{1g}+E_{2g}+A_{2u}+E_{1u}+E_{2u}$
$C_{20}(\text{layer}^j)$	20	0	0	0	0	0	0	0	$A_{1g}+A_{2g}+2E_{1g}+2E_{2g}+A_{1u}+A_{2u}+2E_{1u}+2E_{2u}$

TABLE V. $\chi^{\text{atom sites}}$ for the C_{70+20j} molecules for D_{5h} symmetry.

Site	E	$2C_5$	$2C_5^2$	$5C_2'$	σ_h	$2S_5$	$2S_5^3$	$5\sigma_v$	$\chi^{\text{atom sites}}$
$C_{10}(\text{cap}^0)$	10	0	0	0	0	0	0	2	$A_1'+E_1'+E_2'+A_2''+E_1''+E_2''$
$C_{10}(\text{cap}^1)$	10	0	0	0	0	0	0	2	$A_1'+E_1'+E_2'+A_2''+E_1''+E_2''$
$C_{20}(\text{layer}^j)$	20	0	0	0	0	0	0	0	$A_1'+A_2'+2E_1'+2E_2'+A_1''+A_2''+2E_1''+2E_2''$
$C_{10}(\text{equator})$	10	0	0	0	10	0	0	0	$A_1'+A_2'+2E_1'+2E_2'$

TABLE VI. Vibrational modes of C_{80+20j} molecules with D_{5d} symmetry.

Molecule	A_{1g}[a]	A_{2g}	E_{1g}[b]	E_{2g}[a,b]	A_{1u}	A_{2u}[c]	E_{1u}[c]	E_{2u}	Polarization
$C_{10}(cap^0)$	1		1	1		1	1	1	z
$C_{10}(cap^0)$	1	1	2	2	1	1	2	2	x,y
$C_{10}(cap^1)$	1		1	1		1	1	1	z
$C_{10}(cap^1)$	1	1	2	2	1	1	2	2	x,y
$C_{20}(layer^j)$	1	1	2	2	1	1	2	2	z
$C_{20}(layer^j)$	2	2	4	4	2	2	4	4	x,y
C_{80}	5	2	8	8	3	4	8	8	z
C_{80}	8	8	15	16	8	8	15	16	x,y
C_{80+20j}	$5+j$	$2+j$	$8+2j$	$8+2j$	$3+j$	$4+j$	$8+2j$	$8+2j$	z
C_{80+20j}	$8+2j$	$8+2j$	$15+4j$	$16+4j$	$8+2j$	$8+2j$	$15+4j$	$16+4j$	x,y

[a]Raman-active mode seen in $\|,\|$ polarization.
[b]Raman-active mode seen in $\|,\perp$ polarization.
[c]Infrared-active mode.

atoms. In the limit that j becomes large, the contribution of the caps to the electronic or vibrational spectra becomes negligible. The irreducible representations for the point group D_{5d} contained in $\chi^{\text{atom sites}}$ for C_{60+20j} ($j = 1, 2, \ldots$) are also given in Table IV for each of the unique groupings.

For the case of the C_{50+20j} molecule, the groupings of the atoms are as given by Eq. (3) except for the addition of an equatorial grouping of ten carbon atoms C_{10}(equator). In this case the pentagons connecting the fivefold axis are in phase so that the C_{50+20j} molecule has a horizontal mirror plane. For this case, each of the caps contains 20 carbon atoms. The groupings of the C_{50+20j} molecule

$$C_{10}(cap^0)+C_{10}(cap^1)+C_{10}(equator)+(1+j)C_{20}(layer) \tag{4}$$

are used to determine $\chi^{\text{atom sites}}$ from the symmetry operations for the point group D_{5h} as given in Table V.

For free molecules the symmetries of the vibrational modes are given by the direct product of $\chi^{\text{atom sites}}$ with the irreducible representations of the vector after subtracting off $\chi^{\text{center of mass}}$

$$\chi^{\text{vibrations}} = \chi^{\text{atom sites}} \otimes \chi^{\text{vector}} - \chi^{\text{center of mass}}, \tag{5}$$

where $\chi^{\text{center of mass}}$ indicates that for each molecule it is necessary to subtract off the three degrees of freedom corresponding to $\chi^{\text{translations}}$ and the three degrees of freedom corresponding to $\chi^{\text{rotations}}$. The appropriate irreducible representations contained in χ^{vector} and $\chi^{\text{rotations}}$ are listed in Tables II and III. Listed in Tables VI and VII is the number of times each irreducible representation of D_{5d} and D_{5h} is contained for the various groupings

TABLE VII. Vibrational modes of C_{70+20j} molecules with D_{5h} symmetry.

Molecule	A_1'[a]	A_2'	E_1'[c]	E_2'[a,b]	A_1''	A_2''[c]	E_1''[b]	E_2''	Polarization
$C_{10}(cap^0)$	1		1	1		1	1	1	z
$C_{10}(cap^0)$	1	1	2	2	1	1	2	2	x,y
$C_{10}(cap^1)$	1		1	1		1	1	1	z
$C_{10}(cap^1)$	1	1	2	2	1	1	2	2	x,y
$C_{20}(layer^j)$	1	1	2	2	1	1	2	2	z
$C_{20}(layer^j)$	2	2	4	4	2	2	4	4	x,y
C_{10}(equator)					1	1	2	2	z
C_{10}(equator)	2	2	4	4					x,y
C_{70}	4	1	6	6	3	4	8	8	z
C_{70}	8	8	15	16	6	6	11	12	x,y
C_{70+20j}	$4+j$	$1+j$	$6+2j$	$6+2j$	$3+j$	$4+j$	$8+2j$	$8+2j$	z
C_{70+20j}	$8+2j$	$8+2j$	$15+4j$	$16+4j$	$6+2j$	$6+2j$	$11+4j$	$12+4j$	x,y

[a]Raman-active mode seen in $\|,\|$ polarization.
[b]Raman-active mode seen in $\|,\perp$ polarization.
[c]Infrared-active mode.

of carbon atoms given in Tables VI and VII. The irreducible representations contained in $\chi^{\text{vibrations}}$ for the entire molecules C_{80} and C_{80+20j} as well as C_{70} and C_{70+20j} ($j = 1, 2, \ldots$) are also listed in Tables VI and VII but in these cases, the six degrees of freedom associated with translations and rotations have been subtracted.

2. *Threefold axis*

We now consider the symmetry of the C_{60+18j} ($j = 1, 2, \ldots$) type fibers based on the threefold symmetry axes. (See Tables VIII–XIII.) For j an odd integer the symmetry is D_{3h} with the character table shown in Table XI and for j an even integer the symmetry is D_{3d} with the character table shown in Table VIII. In both cases the $\chi^{\text{atom sites}}$ for the fiber is found from groupings used for the C_{60+18j} molecule

$$C_{12}(\text{cap}^0) + 2C_6(\text{cap}^1) + (2+j)[C_{12}(\text{cap}^0) + C_6(\text{cap}^1)]. \tag{6}$$

This gives rise to $\chi^{\text{atom sites}}$ for the fiber shown in Tables XII and IX for the C_{78+36j} and C_{96+36j} type fibers, respectively, and the corresponding molecular vibrations are shown in Tables XIII and X. Once again, for the full C_{78+36j} and C_{96+36j} ($j = 1, 2, \ldots$) molecules, the six degrees of freedom associated with translations and rotations have been subtracted.

B. Raman- and ir-active modes

The fiber symmetry is lower than that of the icosahedral C_{60} molecule and therefore the infrared- and Raman-active modes associated with the caps are expected to split. We discuss these first. However, for fibers with a large aspect ratio, the most important contributions to the infrared and Raman spectra come from the cylindrical sections because of the much larger number of carbon atoms associated with the cylindrical sections. We discuss these cylindrical section modes second.

Since group D_{5d} is a subgroup of I_h the following splittings of the Raman-active $2A_g + 8H_g$ modes and infrared-active 4 F_{1u} modes occur when the I_h symmetry is lowered to D_{5d} symmetry

$$A_g \rightarrow A_{1g}, \tag{7}$$

$$H_g \rightarrow A_{1g} + E_{1g} + E_{2g}, \tag{8}$$

$$F_{1u} \rightarrow A_{2u} + E_{1u}. \tag{9}$$

In addition to these modes all the even (g) modes derived from the C_{60} molecule become Raman active, but only the A_{2u} and E_{1u} modes are infrared active. The C_{60} modes in the lower D_{5h} symmetry can be identified as

$$A_g \rightarrow A_1', \tag{10}$$

$$H_g \rightarrow A_1' + E_1'' + E_2', \tag{11}$$

$$F_{1u} \rightarrow A_2'' + E_1'. \tag{12}$$

Thus, some polarization selection rules are expected for Raman lines associated with the caps for fibers based on the fivefold axis.

For the graphene tubules related to the threefold axes, all the modes that are even under inversion for D_{3d} symmetry (or under mirror plane reflection for D_{3h}) are Raman active. The same is true for graphene tubules related to the twofold axis. Thus no selection rules other than parity are expected for these cap modes.

In addition to these cap vibrational modes, there will be modes associated with the inserted cylinder. In the limit $j \rightarrow \infty$, these modes give rise to one-dimensional phonon bands which have zone-center Raman- and infrared-active modes. The z axis in the various character tables refers to the axis of highest symmetry (e.g., the fivefold or threefold axes discussed above), and it is along this direction that the one-dimensional phonon and electron bands form. Since this direction is tangential to the rolled up graphene sheet, these phonon modes should be related to graphite in-plane modes, typically observed in the Raman spectra for conventional carbon fibers.

The resulting one-dimensional periodic structure has a unit cell corresponding to one ring of five armchair (or nine zigzag) hexagons. The dispersion relations for the one-dimensional phonon bands will have zone-center ($k_z = 0$) Raman-active and infrared-active modes corresponding to the one-dimensional (1D) Brillouin zone. The direction which is normal to the periodic $\hat{z}$ direction is also tangential to the rolled up graphene layer, so that in-plane graphitic-derived vibrations would be expected in this direction as well. In contrast the radial direction $\hat{\rho}$ normal to $\hat{z}$ and $\hat{\theta}$ for the graphene tubule corresponds to c-axis-derived modes in graphite.

As listed in Tables VI, VII, X, and XIII the $k_z = 0$ modes associated with the cylindrical sections are essentially those containing a factor of j for the table entries. Their mode symmetries can be found by subtracting the modes derived from the cap carbon atoms from the total. In the limit of a fiber with a very large aspect ratio, the cap modes are of vanishing importance. Whereas the tangential modes of the carbon atoms on the cylinder would be expected to have similar mode frequencies to the in-plane phonons of graphite, the radial modes would be expected to be significantly downshifted relative to the c-axis modes in graphite, in analogy to the situation in C_{60}.[13]

C. Dispersion relations

Let us consider the form of the electronic or phonon-dispersion relations for the graphene tubule. A more detailed exposition of the electronic structure for graphene tubules is planned to be published elsewhere.[14] To treat the dispersion relations, we consider the cylindrical coordinates k_ρ, k_θ, and k_z in reciprocal space. Since the fiber surface is a single sheet, there is no dispersion along k_ρ. In the k_θ direction, we have periodic-boundary conditions. For the C_{60+20j} and C_{50+20j} ($j = 1, 2, \ldots$) type fibers, the reciprocal lattice vector in the θ direction is $2\pi/3\hat{a}_0$ where $\hat{a}_0$ is the nearest-neighbor C-C distance, so that by applying the periodic-boundary conditions discussed above, we obtain the size of the reduced reciprocal

TABLE VIII. Character table for the point group D_{3d}.

D_{3d}	E	$2C_3$	$3C_2'$	i	$2S_3$	$3\sigma_d$	Basis functions
A_{1g}	1	1	1	1	1	1	x^2+y^2, z^2
A_{2g}	1	1	−1	1	1	−1	R_z
E_g	2	−1	0	2	−1	0	$\begin{cases}(xz,yz)\\(x^2-y^2,xy)\\(R_x,R_y)\end{cases}$
A_{1u}	1	1	1	−1	−1	−1	
A_{2u}	1	1	−1	−1	−1	1	z
E_u	2	−1	0	−2	1	0	(x,y)

TABLE IX. $\chi^{\text{atom sites}}$ for the C_{96+36j} molecules for D_{3d} symmetry.

Site	E	$2C_3$	$3C_2'$	i	$2S_6^{-1}$	$3\sigma_d$	$\chi^{\text{atom sites}}$
$C_{12}(\text{cap}^0)$	12	0	0	0	0	0	$A_{1g}+A_{2g}+2E_g+A_{1u}+A_{2u}+2E_u$
$C_6(\text{cap}^1)$	6	0	0	0	0	2	$A_{1g}+E_g+A_{2u}+E_u$

TABLE X. Vibrational modes of C_{96+36j} molecules with D_{3d} symmetry.

Molecule	A_{1g}[a]	A_{2g}	E_g[b]	A_{1u}	A_{2u}[c]	E_u[c]	Polarization
$C_{12}(\text{cap}^0)$	1	1	2	1	1	2	z
$C_{12}(\text{cap}^0)$	2	2	4	2	2	4	x,y
$C_6(\text{cap}^1)$	1		1		1	1	z
$C_6(\text{cap}^1)$	1	1	2	1	1	2	x,y
$C_{36}(\text{layer}^j)$	4	2	6	2	4	6	z
$C_{36}(\text{layer}^j)$	6	6	12	6	6	12	x,y
C_{96}	11	4	16	5	10	16	z
C_{96}	16	16	31	16	16	31	x,y
C_{96+36j}	$11+4j$	$4+2j$	$16+6j$	$5+2j$	$10+4j$	$16+6j$	z
C_{96+36j}	$16+6j$	$16+6j$	$31+12j$	$16+6j$	$16+6j$	$31+12j$	x,y

[a] Raman-active mode seen only in $\|,\|$ polarization.
[b] Raman-active mode seen in both $\|,\|$ and $\|,\perp$ polarizations.
[c] Infrared-active mode.

TABLE XI. Character table for the point group D_{3h}.

D_{3h}	E	$2C_3$	$3C_2'$	σ_h	$2S_3$	$3\sigma_v$	Basis functions
A_1'	1	1	1	1	1	1	x^2+y^2, z^2
A_2'	1	1	−1	1	1	−1	R_z
A_1''	1	1	1	−1	−1	−1	
A_2''	1	1	−1	−1	−1	1	z
E'	2	−1	0	2	−1	0	(x,y); (x^2-y^2,xy)
E''	2	−1	0	−2	1	0	(xz,yz) (R_x,R_y)

TABLE XII. $\chi^{\text{atom sites}}$ for the C_{78+36j} molecules for D_{3h} symmetry.

Site	E	$2C_3$	$3C_2'$	σ_h	$2S_3$	$3\sigma_v$	$\chi^{\text{atom sites}}$
$C_{12}(\text{cap}^0)$	12	0	0	0	0	0	$A_1'+A_2'+2E'+A_1''+A_2''+2E''$
$C_6(\text{cap}^1)$	6	0	0	0	0	2	$A_1'+E'+A_2''+E''$

TABLE XIII. Vibrational modes of C_{78+36j} molecules with D_{3h} symmetry.

Molecule	A_1' [a]	A_2'	E' [a,b,c]	A_1''	A_2'' [c]	E'' [b]	Polarization
$C_{12}(cap^0)$	1	1	2	1	1	2	z
$C_{12}(cap^0)$	2	2	4	2	2	4	x,y
$C_6(cap^1)$	1		1		1	1	z
$C_6(cap^1)$	1	1	2	1	1	2	x,y
$C_{36}(layer^j)$	4	2	6	2	4	6	z
$C_{36}(layer^j)$	6	6	12	6	6	12	x,y
C_{78}	9	3	13	4	8	13	z
C_{78}	13	13	25	13	13	25	x,y
C_{78+36j}	$9+4j$	$3+2j$	$13+6j$	$4+2j$	$8+4j$	$13+6j$	z
C_{78+36j}	$13+6j$	$13+6j$	$25+12j$	$13+6j$	$13+6j$	$25+12j$	x,y

[a] Raman-active mode seen in $\|,\|$ polarization.
[b] Raman-active mode seen in $\|,\perp$ polarization.
[c] Infrared-active mode.

lattice vector along k_θ as $2\pi/15\hat{a}_0$. Along the k_z direction, phonon or electronic bands form, and as j becomes large the dispersion along k_z for the fiber should reduce to the in-plane electron or phonon-dispersion relations found on a graphene sheet.

The arguments given above for the dispersion relations for the C_{60+20j} and C_{50+20j} (for $j = 1,2,\ldots$) fibers also apply to the C_{60+36j} and C_{78+36j} fibers except that the length scale along k_θ is now $2\pi/(9\sqrt{3}\hat{a}_0)$.

IV. DISCUSSION

It is interesting to consider a ball-and-stick model of the carbon atoms as they form a fiber. If the carbon atoms are considered as points, the diameter of the C_{60+10j} fiber is $15\hat{a}_0/\pi = 6.83$ Å and the enclosed area is 36.6 Å^2, assuming a C-C distance of $a_0 = 1.43$ Å.[15] If we now consider the graphene sheet in Fig. 2(a) to have a uniform charge distribution extending to $\hat{c}_0/2$ above and below the sheet (where $\hat{c}_0 = 3.35$ Å, the interlayer distance of graphite), then the area on one side of the graphene sheet containing the charge distribution is $15\hat{a}_0\hat{c}_0/2 = 35.9$ Å^2, which is only 2% less than the cross-sectional area of the graphene tubule. The ball-and-stick model thus shows that the fivefold periodic-boundary condition corresponds to the smallest fiber diameter that can contain the electron gas surrounding the graphene sheet, considering the electron gas as an incompressible fluid. This is another way of looking at the C_{60+10j} fiber as an approximation to the fiber of smallest diameter that might be synthesized for a vapor-grown carbon fiber. By introducing chirality into the problem, the overlap of the radially directed orbitals (in the region near the central fiber axis) from opposite sides of the graphene tubule will be reduced by the staggering of the orbitals along the fiber axis direction. This effect may permit a smaller dimension for the minimum diameter fiber, as compared with the case of the armchair and zigzag fibers.

The outer diameter of the armchair fiber can be estimated as 6.83 Å + 3.35 Å = 10.18 Å. However, if we distribute the charge contained in the area $15\hat{a}_0\hat{c}_0/2$ over an annular strip around a circle of diameter 6.83 Å, then the resulting diameter for the C_{60+10j} fiber is only 9.61 Å.

Adding a second layer of carbon atoms around the fiber axis would increase the diameter to 13.66 Å. This second layer would have ten full armchairs, as opposed to five for the first layer, thereby allowing the possibility of fivefold symmetry. Adding and subtracting 3.35 Å to the mean diameter of 13.66 Å yields a rough estimate of 10.31 Å and 17.01 Å for the inner and outer diameters, respectively. If a uniform charge distribution is taken for the inner and outer annular rings, then the resulting inner and outer diameters become 9.75 Å and 16.67 Å, respectively. This estimate is compatible with the 9.61 Å outer diameter of the single layer. Since the area of the charged region above a graphene plane increases proportionally to the length of the super cell in the θ direction and the area enclosed by the cylinder increases as the square of the length, the density of the enclosed charge for graphene tubules derived from the fivefold axis armchair orientation will be slightly more dense than that for the fibers derived from the threefold axis zigzag orientation.

Since it is not possible to build up graphene layers on a curved surface with the $ABAB$ registry of graphite, a turbostratic 2D structure is expected for the cylindrical layers of multilayered graphene-based tubules, suggesting a zero-gap semiconductor for the electronic structure in the limit of large j, in contrast to the 1.8-eV band gap for C_{60}. The possibility of a Peierls distortion forming a small band gap in a one-dimensional periodic structure must also be considered. Carriers could probably be introduced into a graphene tubule by the introduction of dopants within the cylinder of the fiber, by boron substitution for carbon on the cylinder, or by the addition of dopants external to the fiber, as can also be done for C_{60} molecules.[16]

Because of the inherent simplicity of the graphene tubule system, it is expected that these systems will become model systems for the calculation of the mechanical

and electronic properties of idealized carbon fibers, of interest to both the science and application of carbon fibers for practical use.

Recently, there have been two reports of observations of carbon fibers with very small diameters. Iijima[5] using a dc arc discharge from a negatively charged carbon electrode for fiber preparation reported observation of a hollow tubular fiber consisting of only two rolled up graphene sheets and another tubular fiber with an inner diameter of only 23 Å. He claimed that the tubule growth was stabilized by the presence of fiber chirality. Endo,[11] using conventional methods for the preparation of vapor-grown carbon fibers and their subsequent heat treatment to 2800 °C reported the growth of very thin fibers (below 30 Å diameter) out of vapor-grown fibers of larger diameter. Among the small diameter fibers seen by Endo[11] is a hollow fiber with 10.2-Å outer diameter. As the experimental picture for the graphene tubules becomes clarified, appropriate extensions of the present work will be needed to address the symmetry issues, structure, and properties of real carbon fibers with nanometer diameters.

ACKNOWLEDGMENTS

We are grateful to Professor M. Endo, Professor P.C. Eklund, Professor M. Fujita, and Professor R.A. Jishi for their continuing interest in this work. We also acknowledge stimulating discussions with Dr. M. Schluter, Dr. R.L. Whetten, and Dr. S. Iijima. We gratefully acknowledge support by the NSF Grant No. DMR88-19896.

*Permanent address: University of Electro-Communications, Chofu, 182 Tokyo, Japan.

[1] W. Krätschmer, L. D. Lamb, K. Fostiropoulos, and D. R. Huffman, Nature **347**, 354 (1990).

[2] R. E. Haufler, J. J. Conceicao, L. P. F. Chibante, Y. Chai, N. E. Byrne, S. Flanagan, M. M. Haley, S. C. O'Brien, C. Pan, Z. Xiao, W. E. Billups, M. A. Ciufolini, R. H. Hauge, J. L. Margrave, L. J. Wilson, R. F. Curl, and R. E. Smalley, J. Phys. Chem. **94**, 8634 (1990).

[3] G. Meijer and D. S. Bethune, Chem. Phys. Lett. **175**, 1 (1990).

[4] G. Meijer and D. S. Bethune, J. Chem. Phys. **93**, 7800 (1990).

[5] S. Iijima, Nature **354**, 56 (1991).

[6] M. S. Dresselhaus, G. Dresselhaus, K. Sugihara, I. L. Spain, and H. A. Goldberg, *Graphite Fibers and Filaments*, Springer Series in Materials Science Vol. 5 (Springer-Verlag, Berlin, 1988).

[7] R. T. K. Baker and P. S. Harris, in *Chemistry and Physics of Carbon*, edited by P. L. Walker, Jr. and P. A. Thrower (Dekker, New York, 1978), Vol. 14, p. 103.

[8] M. Endo, T. Koyama, and Y. Hishiyama, Jpn. J. Appl. Phys. **15**, 2073 (1976).

[9] J. S. Speck, M. Endo, and M. S. Dresselhaus, J. Cryst. Growth **94**, 834 (1989).

[10] T. C. Chieu, G. Timp, M. S. Dresselhaus, M. Endo, and A. W. Moore, Phys. Rev. B **27**, 3686 (1983).

[11] M. Endo (unpublished).

[12] P. Labastie, R. L. Whetten, H. P. Cheng, and K. Holczer (unpublished).

[13] R. A. Jishi and M. S. Dresselhaus, Phys. Rev. B (to be published).

[14] R. Saito, M. Fujita, G. Dresselhaus, and M. S. Dresselhaus (unpublished).

[15] D. S. Bethune, G. Meijer, W. C. Tang, and H. J. Rosen, Chem. Phys. Lett. **174**, 219 (1990).

[16] Y. Chai, T. Guo, C. M. Jin, R. E. Haufler, L. P. Felipe Chibante, J. Fure, L. H. Wang, J. M. Alford, and R. E. Smalley, J. Phys. Chem. **95**, 7564 (1991).